JOURNAL OF THERMOPHYSICS AND HEAT TRANSFER
Vol. 14, No. 3, July–September 2000

Temperature-Dependent Reflectance of Plated Metals and Composite Materials Under Laser Irradiation

Robert K. Freeman* and Fred A. Rigby†
Science Applications International Corporation, Albuquerque, New Mexico 87111
and
Nicholas Morley‡
U.S. Air Force Research Laboratory, Kirtland Air Force Base, New Mexico 87117

Experiments were performed to investigate laser-heating-induced changes in the surface properties of metals and composite structural materials commonly used in aerospace applications. The objective of this test series was to determine the effect of surface heating on the 1.3-θ m-wavelength laser reflectance of these materials. Reflectance measurements were made using a unique hemiellipsoidal reflectometer. Polished metals, plated metals, and composite materials were tested to determine their temperature-dependent reflectance characteristics in vacuum and air environments. This experiment series produced temperature-dependent, 1.3-θ m laser reflectance curves for use in surface degradation analyses. All of the finishes investigated on duplex stainless-steel substrates increase the low-temperature, 1.3-θ m reflectance compared to the unpolished steel. However, the reflectance decreases dramatically at elevated temperatures when the surfaces discolor. The large reflectance transition observed for the polished and plated steel coupons in air also occur in vacuum. The polished aluminum alloys had a higher 1.3-θ m reflectance than the plated aluminum samples throughout the temperature range. The elevated temperature reflectance of S-glass epoxy is irradiance dependent. Low irradiance creates a black char. A higher irradiance can ignite the char and form a lighter, more reflective surface.

Introduction

DAMAGE to aerospace materials by continuous wave (CW) irradiation from an infrared (IR) laser depends on thermal transfer, resulting from absorption of laser energy by the material. Reflectance is thus a key property for assessing the surface durability of a material. However, under laser illumination conditions, the thermal radiative properties of a material are often not constant. Reflectance, for example, can vary dramatically as a result of thermal decomposition of the surface. Therefore, temperature-dependent reflectance data are needed for accurate computation of laser coupling for surface degradation analyses. Previous prediction algorithms relied solely upon ambient, room temperature reflectance data to determine the thermal response of aerospace materials, often leading to inaccurate results.

The U.S. Air Force Research Laboratory (AFRL) Laser Effects Branch designed and fabricated a unique reflectometer for making real-time measurements of total hemispherical reflectance on samples being heated by front surface irradiation.[1] A number of aerospace materials were tested to determine their temperature-dependent reflectance characteristics in vacuum and air environments. (The in-vacuo tests helped to determine which of the effects observed in the in-air tests were caused by oxidation.)

Temperature-dependent, 1.3-μm laser reflectance curves for polished and unpolished duplex stainless steel, polished and unpolished aluminum alloy, four metallic platings (chromium, two kinds of nickel, and zinc), and composite materials (S-glass/epoxy and carbon phenolic) are presented in this paper.

Presented as Paper 98-2482 at the AIAA 29th Plasmadynamics and Lasers Conference, Albuquerque, NM, 15–18 June 1998; received 8 March 1999; revision received 4 January 2000; accepted for publication 4 January 2000.

*Senior Engineer, Test and Evaluation Group. Associate Fellow AIAA.
†Senior Research Scientist, Technology Integration and Products Group. Member AIAA.
‡Research Engineer, Laser Effects Branch. Member AIAA.

Test Description

Reflectometer

The Laser Effects Test Facility reflectometer is shown in Fig. 1. The interior surface of the reflectometer dome is machined and polished into a hemiellipsoidal shape with a semimajor axis of 173.6 mm and a semiminor axis of 170.4 mm. The sample is placed at one focus of the hemiellipsoid, and the detector is placed at the other. Because the hemiellipsoid acts as a conjugate surface, the laser energy reflected from the sample converges to the detector, regardless of the reflection angle. Figure 2 illustrates the basic principles of reflectometer operation.

A probe beam, having the wavelength for which reflectance measurements are to be made, and a more powerful heater laser beam are directed at the sample through different ports in the reflectometer dome. To minimize heating of the detector, another port in the dome is positioned to allow the specularly reflected part of the heater beam to escape. The plane of incidence of the probe beam is orthogonal to that of the heater beam to minimize loss of scattered probe beam energy through this port. Use of the heater beam allows measurements using front surface heating without requiring a powerful laser for each wavelength to be investigated. The probe beam, which has a smaller diameter than the heater beam, is directed at the center of the sample to ensure that the reflectance measurement is made on an area that is effectively isothermal.

An electrical heater block can be placed behind the sample for supplemental heating. Like the heater laser, its output can be varied to achieve a gradual heat-up rate. The heater block also reduces rear surface reradiation losses. It was used during most of the steel sample tests and for some of the more reflective aluminum samples, to reach higher maximum temperatures. The heater block was not used in the composite materials tests.

There is also a port in the dome that allows direct measurement of the probe beam specular reflectance. A reflective plug can be inserted into this port to take total reflectance measurements using only the meter inside the dome.

The ports can be sealed with transmissive windows, and the dome can be evacuated for in vacuo testing. The area of these openings is small compared to the surface area of the dome, and reflectance

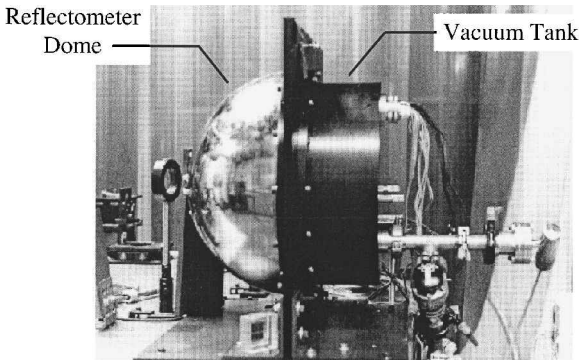

Fig. 1 LETF reflectometer.

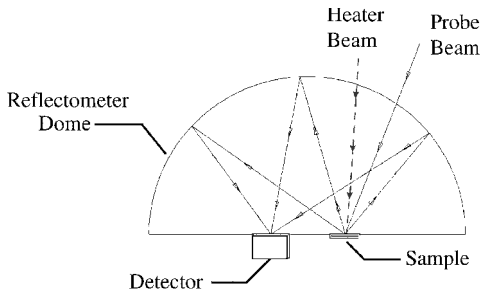

Fig. 2 Reflectometer optics principles.

calibration measurements are performed with the port windows or plugs in the same configuration used in the reflectance test. For the in-vacuo tests of metals, the pressure inside the reflectometer was typically 0.2 torr at the beginning of a test and 0.15 torr at the end. A vacuum roughing pump ran throughout the tests on metal samples, including during sample cooldown. It was turned off during the in vacuo irradiation of the composite materials to avoid contaminating the pump. The pressure inside the reflectometer increased (mainly due to sample outgassing) to around 5 torr during a temperature-dependent reflectance test of S-glass epoxy and to 12–14 torr for a test of carbon phenolic.

The dome is made of 6061 T6 aluminum alloy with an electroless nickel reflective plating on the inner surface. The hard nickel surface can be cleaned repeatedly without scratching. This is necessary because significant surface contamination can accumulate during tests of materials that char (e.g., S-glass epoxy). Unlike an integrating sphere, energy reaches the detector after only a single reflection from the surface of the dome so that there is minimal sensitivity to contaminant accumulation during a single test. For the in-air tests a low-velocity fan was used to exhaust smoke through a hole in the baseplate to eliminate most contamination of the dome surface. Reference 1 describes the design and fabrication of the reflectometer in more detail.

Other hemiellipsoidal reflectometers have been utilized for different applications. Wood et al. developed a hemiellipsoidal reflectometer for the U.S. Air Force Arnold Engineering Development Center.[2,3] It placed the radiation source (a diffuse blackbody) at one focus of the hemiellipsoid to provide diffuse illumination of a test sample located at the other focus. A hole was cut in the dome to pass radiation reflected from the sample to a spectrometer. This device was used to make in situ spectral (2–25 μm) reflectance measurements of mirrors that were cooled to cryogenic temperatures, with and without condensed gas contaminants.[4] A similar device was developed by Surface Optics Corporation, San Diego, California, to make room-temperature directional reflectance measurements.[5]

Antropix Corporation, Woodlands, Texas, used an integrating sphere mounted in a vacuum chamber to measure temperature-dependent reflectance, primarily for satellite thermal control coatings.[6] Their test coupons were held in a resistively heated sample holder (not heated by a laser).

Laser Beamtrains and Instrumentation

The temperature-dependent reflectance measurements used a 1.3-μm, Nd:YAG laser as the probe beam and a 1.06-μm, Nd:YAG laser as a heater beam. Room-temperature reflectance measurements, taken prior to the temperature-dependent reflectance tests, used the 1.3-μm probe beam only. The 6-W, quasi-Gaussian probe beam was chopped at ~3 Hz to create a 0.016-s-wide pulse. It was apertured to a 6 mm wide × 8 mm high oval-shaped spot. The heater laser was operated in CW mode at ~50 W, with a quasi-Gaussian beam profile. Most tests used an oval-shaped heater laser spot that was focused to about 12 mm wide × 16 mm high.

Three joulemeters were used in the reflectance tests and calibrations. All of the meters were positioned after the chopper wheel in the probe laser beamtrain (i.e., they measured a pulsed signal). A Coherent LMP5 joulemeter was used to measure the reference signal reflected from a quartz beam splitter (~7% split off of the probe laser beam) just prior to beam entry into the reflectometer dome. (The reference signal pulse height is proportional to the pulsed probe beam energy incident on the sample.) A Molectron J50 joulemeter was located outside the dome's 2-cm-diam probe beam specular reflectance port. Another Molectron J50 joulemeter was positioned inside the dome, mounted in the dome baseplate at the detector focus of the hemiellipsoid. The dome meter collects reflected energy that does not exit through the specular port. (For some tests a reflective plug was placed in the specular port so that the specular reflection could also be focused to the dome detector.) Two Coherent thermopile meters were also used. One measured the CW probe laser output power that was reflected from a quartz splitter, in front of the chopper wheel. The other thermopile meter monitored heater laser power, also reflected from a quartz splitter.

Video was taken through the heater beam entry port. When recording at visible wavelengths (i.e., for most tests of metal samples), a 1.06-μm filter was mounted in front of the camera lens to eliminate a green glare produced by backscatter of the heater laser wavelength off the sample. During tests of composite material samples and some metal samples, a Hughes IR (3–5-μm) camera collected front surface temperature data, also through the heater beam entry port. The video camera and IR camera were never used simultaneously.

Calibration and Data Reduction

Pretest and posttest calibrations were made to account for the 1.3-μm absorptance of the nickel-plated reflecting surface of the reflectometer dome interior, any increase in absorptance caused by surface contamination on the dome and windows during a test, and losses through the ports. Specular calibrations used a coated glass mirror that has a reflectivity of 99% at 1.3 μm. The dome meter was calibrated with the specular port plug in (referred to as the specular calibration for dome meter in the reflectance plots). The specular port meter was calibrated with the plug out and the sapphire window in place (referred to as the specular plug out calibration for the specular port meter in the plots). The diffuse calibrations were performed with all reflectometer dome windows and/or port plugs in place (as in the reflectance test configuration). Diffuse calibration measurements were made for each reflectance test using three, isotropically diffuse, Labsphere Spectralon calibration standards with 1.3-μm reflectances of 99.1, 80.2, and 62.0%.

The specular and diffuse calibration values showed that there was no significant contamination of the dome surface for the data presented in this paper (metals tested in air and in vacuum and composites tested in air). For these experiments the pretest calibrations were very close to the posttest calibrations (differences were much less than 1%). This is well within the repeatability of the instrument measurements, and so it was not necessary to make any corrections for accumulation of soot, etc., on the dome.

The reflectance calibration factor is the ratio of the reflectance joulemeter pulse height to the reference joulemeter pulse height, normalized to reflectance of the calibration object, and averaged over all pulses in the reflectance calibration data file (typically 30 s, or ~90 pulses).

Reflectance of a sample during a test is then calculated as the ratio of the reflectance joulemeter pulse height to the reference joulemeter

pulse height, divided by the calibration factor. Total reflectance is the sum of the reflectances measured by the dome meter and the specular port meter.

Test Samples

All of the samples were nominally 19.1 × 19.1 mm square. Two Chromega/Alomega type K thermocouple (TC) probes were used to measure sample rear surface temperature during the tests. Each test had one TC located at the center of the sample. A second TC, referred to as the mid TC, was positioned at the midpoint along the diagonal between the center and the lower-right-hand corner of the coupon.

Metals

Nine duplex stainless-steel coupons were fabricated from each 2-mm-thick, 63.5 × 63.5 mm blank. Unpolished (a baseline case for comparison purposes), mechanically polished, and electropolished samples were tested. The electropolishing solution was Hydrite 2500. The mechanical polishing was a four-step process: 1) rough wheel, 2) Lea compound, 3) Sisal wheel, and 4) color buffing wheel. In addition, some samples were first mechanically polished, then electropolished. It was expected that this would produce something approaching the maximum reflectance achievable from polishing. Similarly, three electroplated surfaces (chromium, nickel, and zinc) were tested to find out which plating material would provide the highest IR reflectivity. Prior to plating, one side of each blank was mechanically polished. A large majority of these plated samples were later tested by irradiating the polished side. Others were irradiated on the unpolished side. All chrome-plated samples (steel and aluminum) were flash coated with nickel before being chrome plated. This is standard practice for chrome electroplating. It gives much better adhesion to the substrate and provides a visibly brighter finish. The plating thickness (on all substrates) was ~0.025 mm.

Three types of aluminum alloys were tested: 1) 2024-T3, clad with pure aluminum; 2) 6061-T6; and 3) 7075-T6. The aluminum coupons were cut from 63.5 × 63.5 mm blanks, which had been cut from a single sheet of each type of aluminum. The sheet thicknesses were 1.3 mm for the 2024-T3, 1.5 mm for the 6061-T6, and 1 mm for the 7075-T6 aluminum. The coupon preparations were similar to those discussed for stainless steel, with two exceptions. First, the aluminum coupons were not electropolished because no vendors in the Albuquerque area could electropolish aluminum. Second, none of the aluminum coupons were zinc plated because a toxic reaction product is generated. Instead, some of the aluminum samples were given an electroless nickel plating. Table 1 summarizes the various metal surface treatments investigated in this study.

Composites

Three types of composite materials were tested: 1) nine plies (total thickness ~4.0 mm) of rayon MX 4926 precursor carbon phenolic bonded to 2-mm-thick duplex stainless steel; 2) five to six plies (total thickness ~3.5 mm) of polyacrylonitrile (PAN) MX 4920 precursor carbon phenolic bonded to 2-mm-thick duplex stainless steel; and 3) eight to nine plies (~5.8 mm total thickness) S-glass epoxy.

Table 1 Surface treatments for duplex stainless-steel and aluminum substrates

Substrate(s)	Polish	Plate
All metals	Unpolished	None
All metals	Mechanically polished	None
Duplex stainless steel	Electropolished	None
Duplex stainless steel	Mechanically polished, then electropolished	None
Duplex stainless steel	Unpolished	Chrome electroplate
All metals	Mechanically polished	Chrome electroplate
Duplex stainless steel	Unpolished	Nickel electroplate
All metals	Mechanically polished	Nickel electroplate
All aluminums	Mechanically polished	Electroless nickel
Duplex stainless steel	Unpolished	Zinc electroplate
Duplex stainless steel	Mechanically polished	Zinc electroplate

There were two distinctly different batches of the S-glass epoxy samples, each composed of eight to nine plies. The first batch (referred to as batch A) had a void fraction (as a percentage of volume) of 2.49 ± 0.50%. The void fraction of the second batch (batch B) was greater, 8.36 ± 0.45%. Batch B was visibly lighter colored, and the layup pattern was more clearly seen than in batch A because of light scattering by the larger voids.

Results of Laser Reflectance Experiments

Room-Temperature Reflectance Tests

Over 100 room-temperature 1.3-μm reflectance tests were performed. Measurements were taken for multiple samples of each kind of surface preparation (typically 5 to 10 test coupons of each type). The data are summarized in Tables 2–6 as the mean value for all of the samples, plus or minus the standard deviation from the mean. The minimum and maximum values are given in parentheses. The results are consistent with database[7] and handbook[8] values. The reflectance values obtained for three of the unpolished duplex steel samples were each verified (within 1%) by AFRL Optical Component Evaluation Laboratory technicians using an integrating sphere.[9] The repeatability of the reflectometer measurements is approximately ±1%.

Duplex Stainless Steel

Table 2 gives results of the room temperature reflectance measurements for the duplex stainless-steel coupons.

Aluminum Alloys

Tables 3–5 summarize the room-temperature measurements for aluminum alloys.

Composite Materials

The room-temperature reflectance values for the composite material coupons are given in Table 6. The S-glass epoxy virgin material

Table 2 Room-temperature 1.3-θ m total hemispherical reflectance of duplex stainless-steel samples

Polish	Electroplate	Reflectance (%)
Unpolished	None	44 ± 4 (37–49)
Mechanical	None	61 ± 1 (59–63)
Electropolished	None	68 ± 2 (63–72)
Mechanical, then electropolished	None	69 ± 2 (66–70)
Unpolished	Chrome	64 ± 2 (62–66)
Mechanical	Chrome	66 ± 1 (64–68)
Unpolished	Nickel	72 ± 2 (70–74)
Mechanical	Nickel	77 ± 4 (72–83)
Unpolished	Zinc	83 ± 3 (78–87)
Mechanical	Zinc	84 ± 1 (82–85)

Table 3 Room-temperature 1.3-θ m total hemispherical reflectance of aluminum-clad 2024-T3 aluminum alloy samples

Polish	Electroplate	Reflectance (%)
Unpolished	None	76 ± 4 (72–79)
Mechanical	None	94 ± 2 (92–97)
Mechanical	Chrome	66 ± 2 (64–68)
Mechanical	Nickel	79 ± 4 (75–84)

Table 4 Room-temperature 1.3-θ m total hemispherical reflectance of 6061-T6 aluminum alloy samples

Polish	Plate	Reflectance (%)
Unpolished	None	70 ± 1 (69–71)
Mechanical	None	93 ± 4 (90–96)
Mechanical	Chrome electroplate	65 ± 2 (64–68)
Mechanical	Nickel electroplate	74 ± 2 (71–77)
Mechanical	Electroless nickel	72 ± 2 (70–75)

Table 5 Room-temperature 1.3-θ m total hemispherical reflectance of 7075-T6 aluminum alloy samples

Polish	Plate	Reflectance (%)
Unpolished	None	70 ± 2 (69–72)
Mechanical	None	92 ± 3 (91–97)
Mechanical	Chrome electroplate	67 ± 2 (65–70)
Mechanical	Nickel electroplate	74 ± 4 (70–80)
Mechanical	Electroless nickel	73 ± 2 (71–76)

Table 6 Room-temperature 1.3-θ m total hemispherical reflectance of composite material samples

Material	Reflectance (%)
S-glass epoxy batch A	27 ± 2 (25–30)
S-glass epoxy batch B	47 ± 2 (44–49)
PAN precursor carbon phenolic	7.0 ± 0.2 (6.7–7.5)
Rayon precursor carbon phenolic	6.0 ± 0.1 (5.8–6.1)

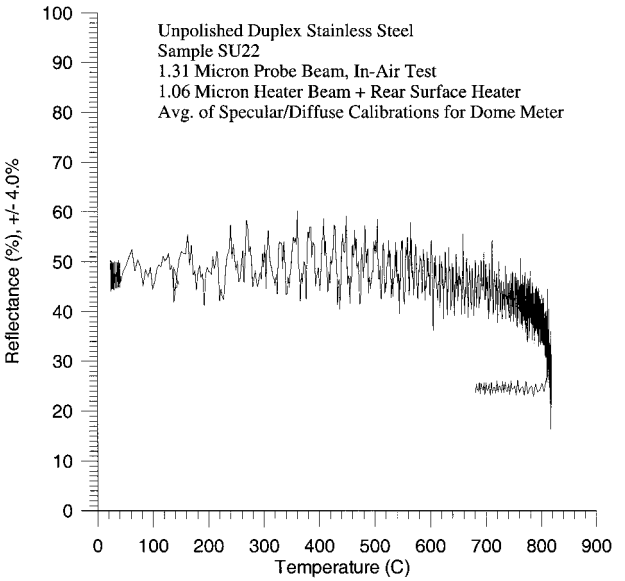

Fig. 3 Temperature-dependent 1.3-θ m total hemispherical reflectance of unpolished duplex stainless steel.

samples transmit much of the incident 1.31-μm laser energy (~34% for the batch A samples and 15% for batch B).

Temperature-Dependent Reflectance Tests

Over 100 temperature-dependent reflectance tests were conducted. A large majority of the tests were in air. At least one of each sample type was tested in vacuum. Three or more temperature-dependent tests were performed for each type of metal surface finish and for each composite material.

Duplex Stainless Steel

The steel samples reached maximum temperatures of over 800°C. (Many exceeded 900°C.) This is well below the melting point for stainless steel (~1477°C), nickel (1453°C), and chromium (1875°C) but higher than the melting point of zinc (419°C). The maximum temperatures achieved also surpassed the temperature necessary to initiate crystalline phase change on the steel surface (550–600°C).

Figures 3–9 are examples of temperature-dependent reflectance plots for in-air tests of the various combinations of surface polishes and platings on a duplex stainless-steel substrate. Reflectance is plotted against the center TC temperature, unless noted otherwise. Most of the curves exhibit little change over the first few hundred degrees of sample heating, followed by an increasingly steep drop in reflectance. The lowest reflectance usually occurs at the maximum

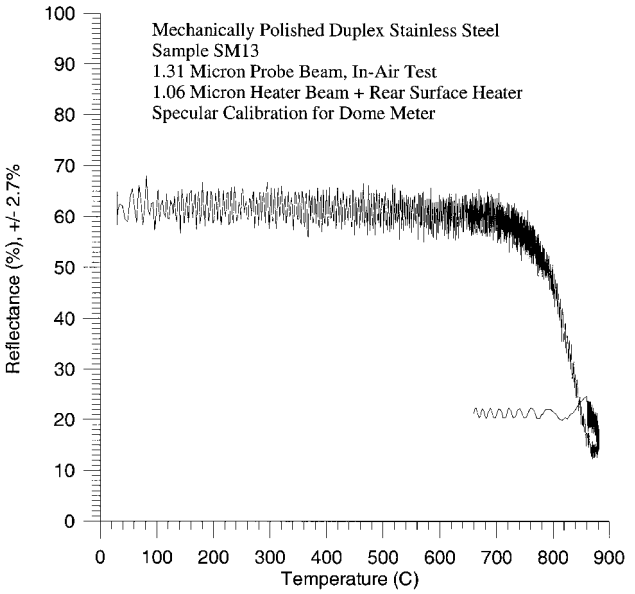

Fig. 4 Temperature-dependent 1.3-θ m total hemispherical reflectance of mechanically polished duplex stainless steel.

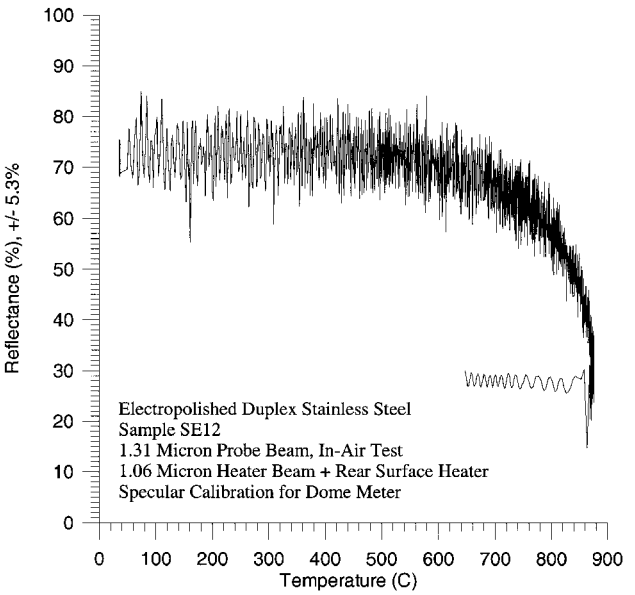

Fig. 5 Temperature-dependent 1.3-θ m total hemispherical reflectance of electropolished duplex stainless steel.

temperature achieved, which is the point at which the heat losses equal the combined input from the heater laser and the rear surface heater. Most plots include reflectance data taken while the sample cools from ~900°C down to ~600°C, after the temperature levels out and heating has been discontinued. Reflectance remains low during the cooldown period, although there is a small recovery in some cases. For other samples, there does not appear to be any recovery.

All of the plots exhibit some noise caused by scatter of reflected 1.06-μm heater beam energy, which is reimaged to the dome meter. Initially, temperature-dependent reflectance tests were performed on the same types of duplex stainless-steel coupons using a 10.6-μm heater laser that had a much more stable power supply. The data plots for these tests were virtually noise free, and the curves agreed closely with the mean values of the data presented in Fig. 3. The 1.06-μm heater laser was used for most of the experiments because the 10.6-μm laser did not have sufficient output power to heat the samples to the desired maximum temperatures.

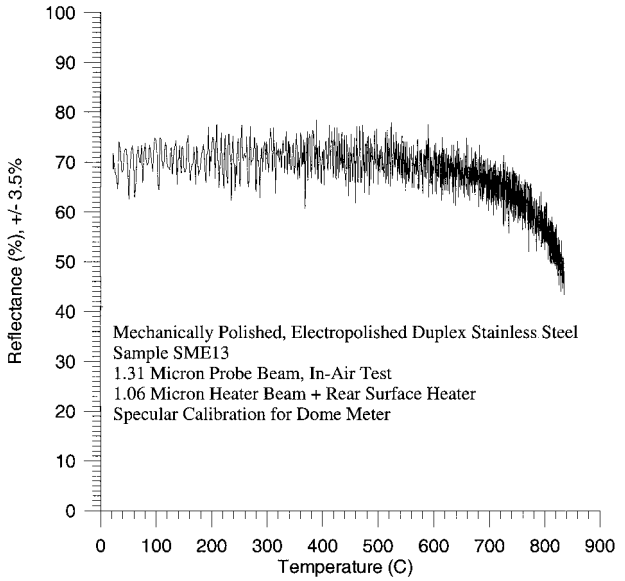

Fig. 6 Temperature-dependent 1.3-θm total hemispherical reflectance of mechanically polished/electropolished duplex stainless steel.

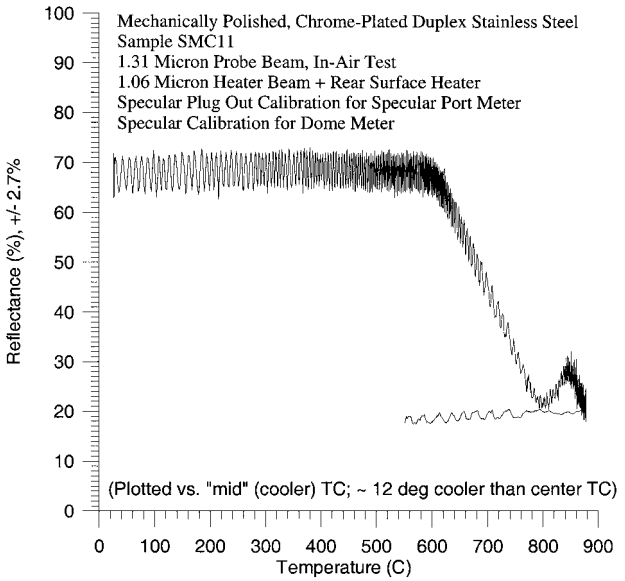

Fig. 7 Temperature-dependent 1.3-θm total hemispherical reflectance of mechanically polished, chrome-electroplated duplex stainless steel.

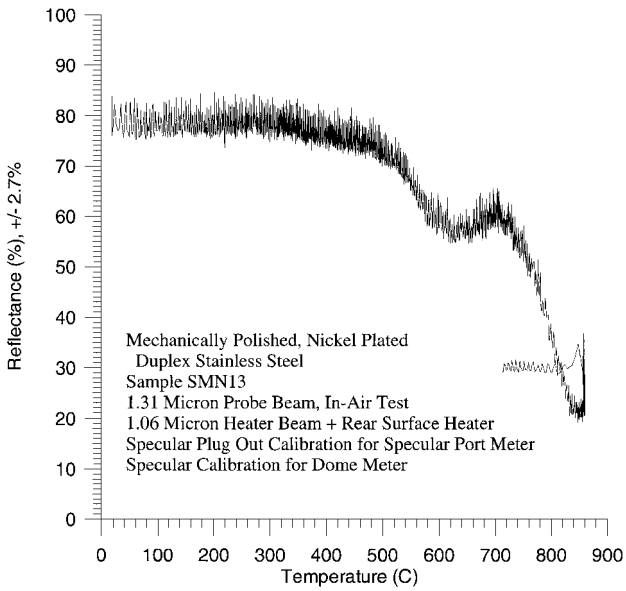

Fig. 8 Temperature-dependent 1.3-θm total hemispherical reflectance of mechanically polished, nickel-electroplated duplex stainless steel.

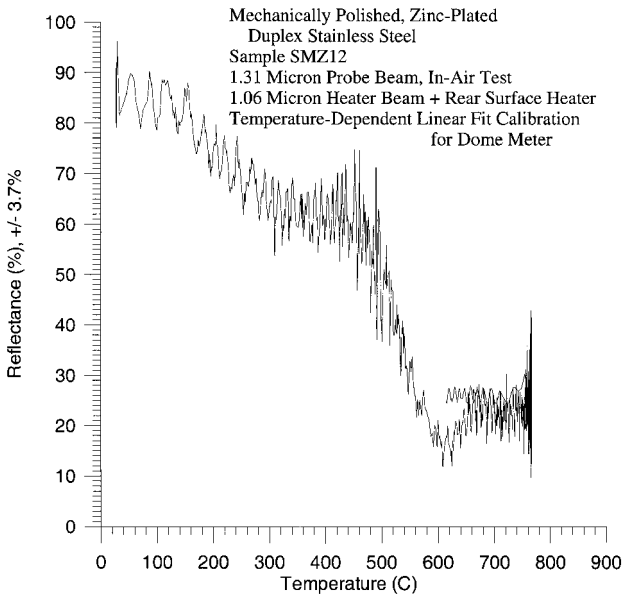

Fig. 9 Temperature-dependent 1.3-θm total hemispherical reflectance of mechanically polished, zinc-electroplated duplex stainless steel.

The reflectance measurement uncertainty listed in each plot is a measure of the noise in the data. It is calculated as the standard deviation from the mean across a temperature range where the curve is relatively flat. The temperature-dependent reflectance measurements for the unpolished steel (Fig. 3) agree within 5% of high-temperature calorimetric coupling values for this material from earlier AFRL experiments. The temperature measurement uncertainty is defined by the manufacturer of the TCs (Omega Engineering, Inc., Stamford, Connecticut) to be the greater of 2.2°C or 0.75% of the measurement.

The bare steel, when tested in air, starts to turn brown because of oxidation at just over 400°C (Figs. 3–6). This results in a small decrease in reflectance. The major transition to lower reflectance (over 600°C) is apparently caused by the crystalline phase change, which causes the surface to turn a dark blue-purple tint, mixed with brown oxidation.

The chrome plating (Fig. 7) and nickel plating (Fig. 8) also darken at high temperatures, greatly decreasing 1.3-μm reflectance. These two platings remained intact, with no signs of cracking or flaking. The zinc plating melts off at ~420°C and leaves a very thin film of zinc oxide powder (Fig. 9). A large decrease in reflectance occurs as the probe laser shines through to the darkened steel beneath the zinc oxide.

For the plated samples there was not a great difference between the surface durability and reflectance of coupons irradiated on the unpolished side (not plotted here) and the coupons irradiated on the polished side (Figs. 7–9).

The in-vacuo tests were performed to help to determine which of the effects observed in the in-air tests were caused by oxidation. The large temperature-dependent change in reflectance observed in air also occurs in vacuum. Thus, this effect does not seem to be associated with the presence of oxygen. However, the transition tends to be somewhat steeper in vacuum, and a lower reflectance is often achieved. Figure 10 is the temperature-dependent reflectance of an unpolished duplex stainless-steel sample tested in vacuum (compare to the in-air test of an unpolished sample, Fig. 3). The steel samples tested in vacuum had a cleaner posttest appearance than those tested in air. The blue-purple tint associated with the crystalline phase change is more pronounced on the steel samples tested in vacuum.

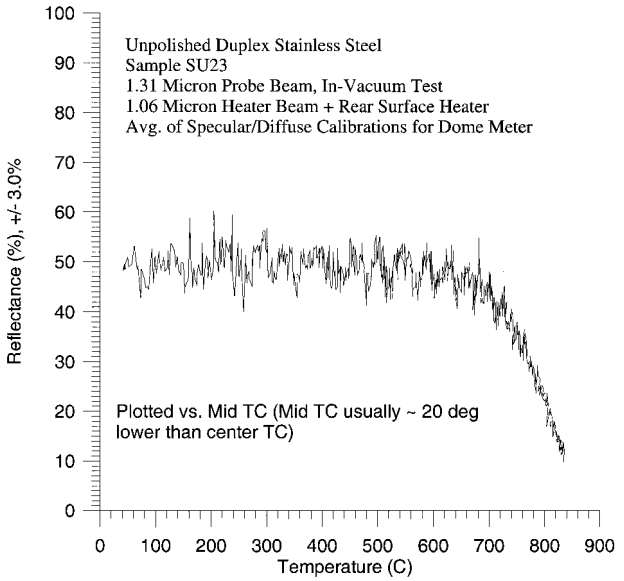

Fig. 10 Temperature-dependent 1.3-θ m total hemispherical reflectance of unpolished duplex stainless steel, in-vacuum test.

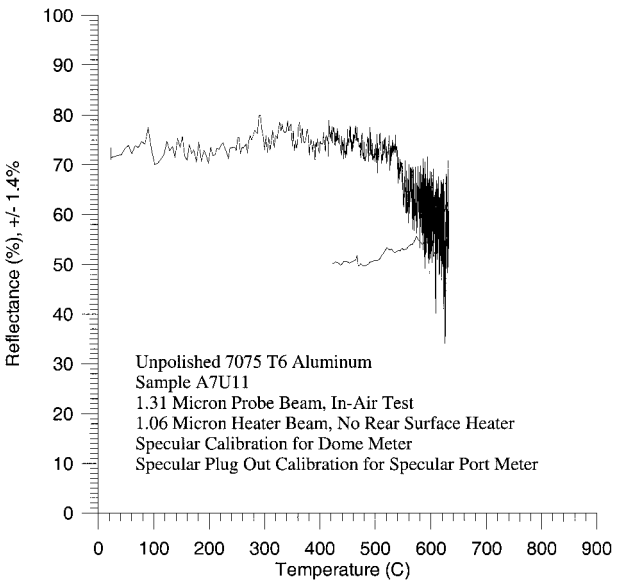

Fig. 11 Temperature-dependent 1.3-θ m total hemispherical reflectance of unpolished 7075-T6 aluminum alloy.

Aluminum Alloys

The aluminum alloy samples were heated to their melting points, which are far below the melting points of the platings. The solidus and liquidus, respectively, for the alloys tested are the following: 502°C and 638°C for 2024 aluminum (660°C for the pure aluminum cladding over the 2024 aluminum); 582°C and 652°C for 6061 aluminum; and 477°C and 635°C for 7075 aluminum.[10] Figures 11–14 are examples of temperature-dependent reflectance plots for in-air tests of the various surface polishes and platings on a 7075-T6 aluminum alloy substrate. Tests of the 6061 and 2024 aluminum samples gave similar results. The thermocouples mounted on the rear surface of the samples seemed to give faulty readings (sometimes higher than the liquidus temperature) after the aluminum substrate began to melt.

The bare aluminum samples (Figs. 11 and 12) darkened slightly prior to melting of the substrate. The bare aluminum was usually a dark silver color at the end of the test.

The chrome plating (Fig. 13) was often blue-purple with yellow blisters after the sample began to melt, whereas the nickel (Figs. 14 and 15) turned black. The nickel reflectance began to decrease at

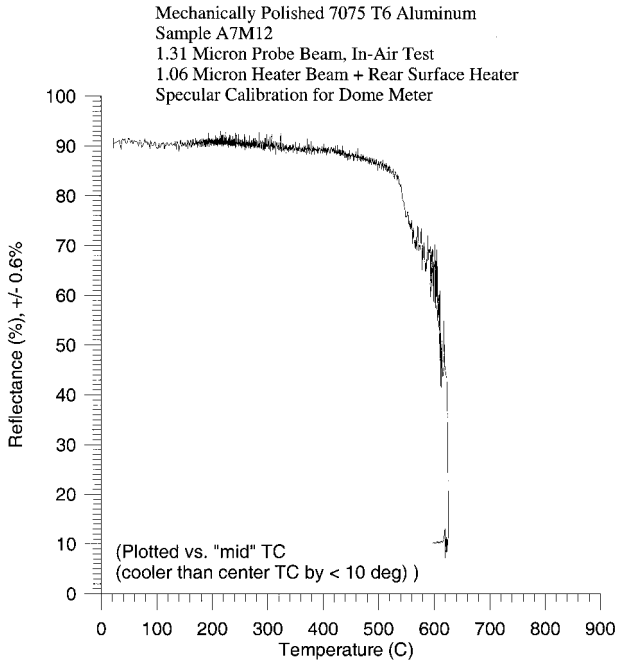

Fig. 12 Temperature-dependent 1.3-θ m total hemispherical reflectance of mechanically polished 7075-T6 aluminum alloy.

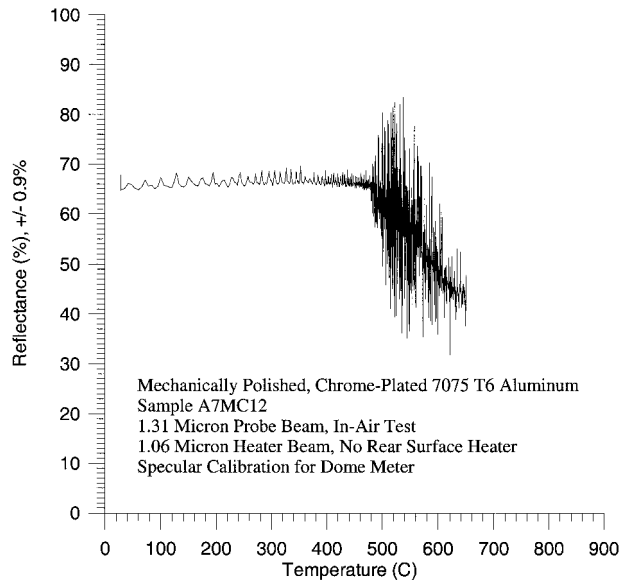

Fig. 13 Temperature-dependent 1.3-θ m total hemispherical reflectance of mechanically polished, chrome-electroplated 7075-T6 aluminum alloy.

~350–400°C, just as in the tests of nickel-plated steel. Violent reactions caused by outgassing (blisters forming and bursting) were observed during tests of some of the plated samples.

Composite Materials

In air and in vacuum the S-glass epoxy samples showed a large increase in reflectance (back scatter) prior to charring. This seems to result from a growing void space between the fibers and epoxy as the samples expand because of laser heating. The sample color changes from yellow/gold (virgin material) to a milky white. In air the coupons heated with a higher irradiance (27 W/cm^2) charred, then ignited, with flames visible for several seconds. The surface was a silver-white color posttest. It was opaque to 1.3-μm radiation. The front surface temperature of the samples exceeded 950°C (the saturation temperature of the IR camera) while the sample was burning. The samples heated with a lower irradiance in air (stepped

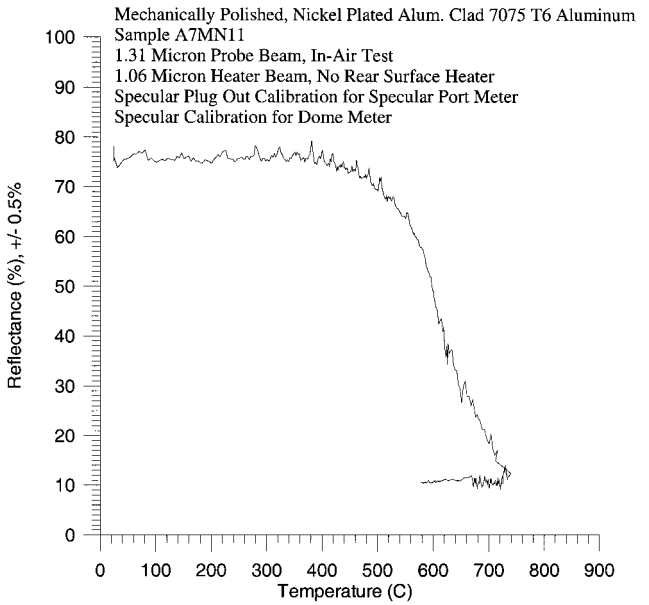

Fig. 14 Temperature-dependent 1.3-θ m total hemispherical reflectance of mechanically polished, nickel-electroplated 7075-T6 aluminum alloy.

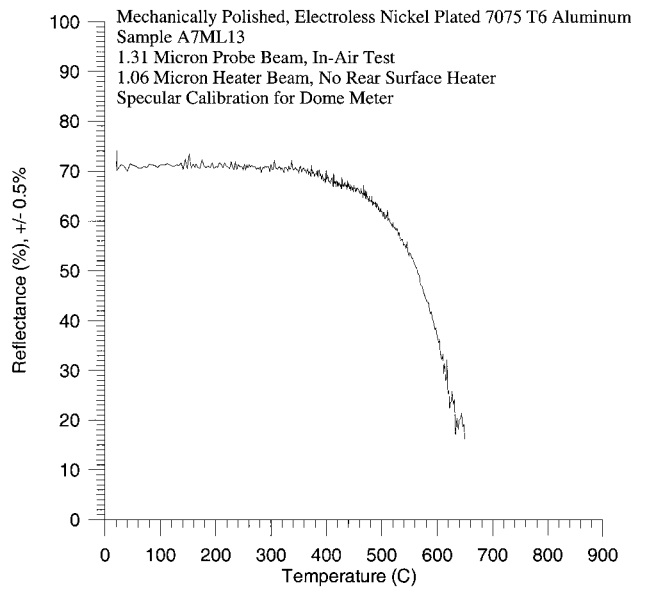

Fig. 15 Temperature-dependent 1.3-θ m total hemispherical reflectance of mechanically polished, electroless nickel-plated 7075-T6 aluminum alloy.

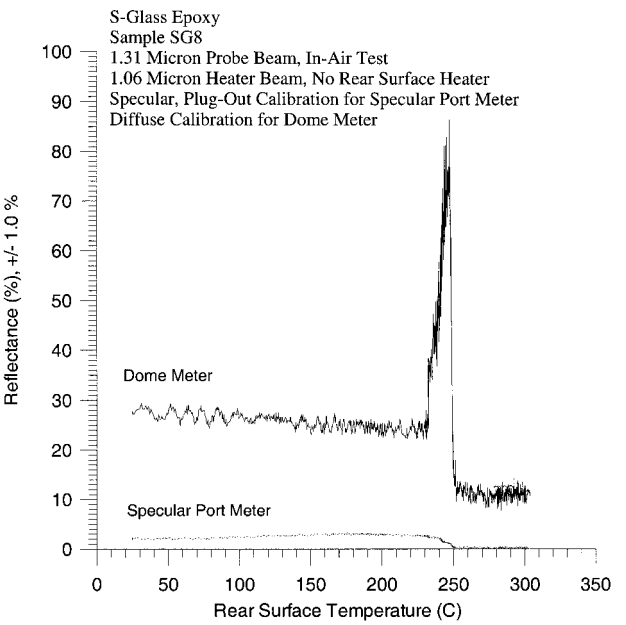

Fig. 16 The 1.3-θ m total hemispherical reflectance vs rear surface temperature for batch A s-glass epoxy (low irradiance: char did not ignite).

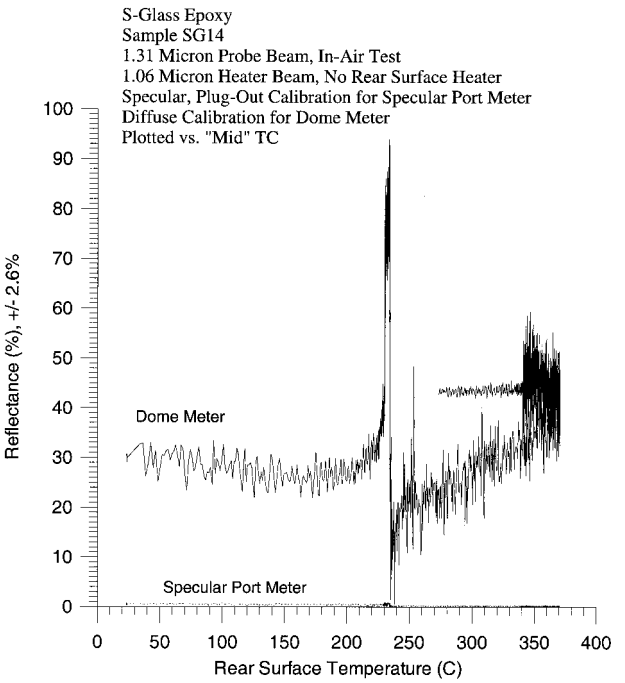

Fig. 17 The 1.3-θ m total hemispherical reflectance vs rear surface temperature for batch A s-glass epoxy (higher irradiance: char ignited).

up from 8 to 24 W/cm^2 over 300 s) charred without burning, producing a glossy black char. The maximum front surface temperature for these samples was about 800°C. (The samples heated in vacuum also formed a glossy black char.) Figure 16 is a plot of reflectance vs rear surface temperature for a sample that did not ignite after charring, whereas Fig. 17 is the same type plot for a sample that did ignite. (For these two plots the total hemispherical reflectance is the sum of the measurements of the dome meter and the specular port meter.) As would be expected, the silver-white surface on the sample that ignited has a much higher 1.3-μm reflectance than the black char on the sample that did not ignite. Posttest examination showed that a small amount of ply delamination occurred. Both batches of S-glass charred and ignited at about the same temperatures.

The PAN precursor carbon phenolic always debonded from the steel substrate, whereas only a couple of the rayon precursor carbon phenolic samples debonded. A sufficient amount of resin baked out to reveal the fibers. The remaining resin was visibly a little lighter colored than on the virgin material. Front surface temperatures surpassed 850°C. In Fig. 18 the reflectance of a PAN fiber carbon phenolic sample is plotted vs rear surface temperature. This sample was tested in air. The temperature-dependent reflectance behavior of the rayon precursor carbon phenolic was very similar to that shown in Fig. 18. The carbon phenolic samples tested in vacuum also showed a gradual increase in reflectance as they were heated. The magnitude of the increase was similar to the in-air data.

Linear Fit Temperature-Dependent Reflectance Models

For surface degradation analyses piecewise linear curves (models) approximating the characteristic reflectance behavior of the various metal and composite surfaces can be developed from the

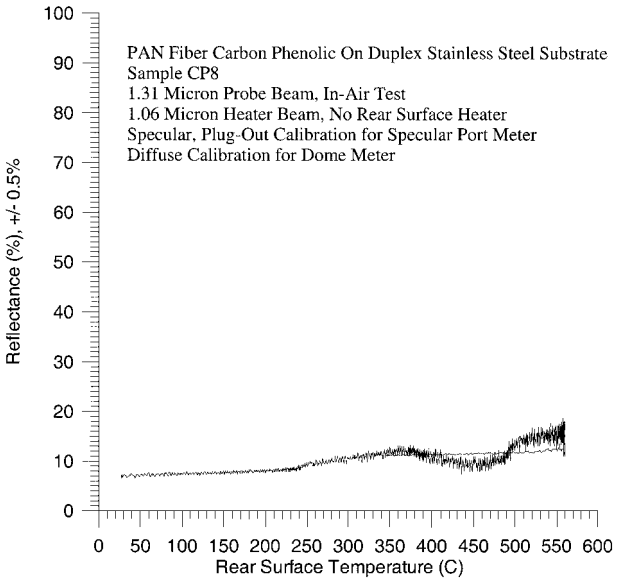

Fig. 18 The 1.3-θm total hemispherical reflectance vs rear surface temperature for PAN fiber precursor carbon phenolic.

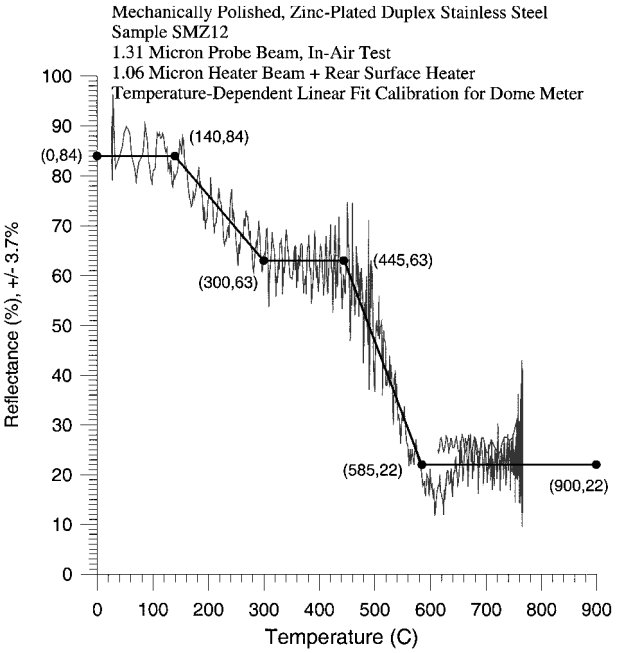

Fig. 19 Temperature-dependent 1.3-θm reflectance model for zinc-plated, mechanically polished duplex stainless steel.

temperature-dependent reflectance data. The general phenomenology is determined from multiple tests of each sample type. The most important priorities are to accurately select 1) the starting point (room-temperature reflectance); 2) the temperatures at which the major reflectance transitions begin and end; and 3) the end point (high temperature reflectance). It is also desired to represent the behavior over the room temperature-to-transition temperature range reasonably well, but without attempting to duplicate the minor (and highly variable) bumps and wiggles displayed by individual curves. Figure 19 is an example of a piecewise linear fit determined from multiple sets of data. For this plot the linear fit is drawn through the data from a test of a duplex stainless-steel coupon that was electroplated with zinc. The model also closely matches the data from another test of an identically prepared sample.

Conclusions

All of the finishes investigated on duplex stainless-steel substrates increase the low-temperature, 1.3-μm reflectance compared to the unpolished steel. However, the reflectance decreases dramatically at elevated temperatures when the surfaces discolor. This occurred regardless of the surface preparation, although some of the finishes (e.g., nickel electroplate and electropolished steel) performed better than others at higher temperatures. For the plated samples there was little difference between the surface durability and reflectance of coupons irradiated on the unpolished side and those irradiated on the polished side.

The large reflectance transition observed for the polished and plated steel coupons in air also occur in vacuum. The transition tends to be somewhat steeper in vacuum, and a lower reflectance is often achieved.

For the aluminum alloys the polished surfaces had a higher 1.3-μm reflectance than the plated finishes throughout the temperature range. The plated aluminum behaved much like the steel samples plated with the same materials up to the solidus temperature of the aluminum.

A small, gradual increase in 1.3-μm reflectance occurs for the carbon phenolic samples, beginning shortly after the start of irradiation by the heater beam. The elevated temperature reflectance of S-glass epoxy is irradiance dependent. Low irradiance creates a black char. A higher irradiance can ignite the char and form a lighter, more reflective surface.

Acknowledgments

This work was performed for the Laser Effects Branch of the Air Force Research Laboratory at Kirtland Air Force Base, New Mexico. The authors wish to acknowledge the test support of James Householder, The Boeing Company.

References

[1]Ward, D. B., Grimes, L. E., Freeman, R. K., Doerr, S. E., Rigby, F. A., and Householder, J., "Temperature-Dependent Reflectance of Aerospace Materials," Air Force Research Lab., Final Rept., PL-TR-97-1059, Kirtland AFB, NM, May 1997.

[2]Wood, B. E., Pipes, J. G., Smith, A. M., and Roux, J. A., "Hemi-Ellipsoidal Mirror Infrared Reflectometer: Development and Operation," *Applied Optics*, Vol. 15, No. 4, 1976, pp. 940–950.

[3]Wood, B. E., Pipes, J. G., Smith, A. M., and Roux, J. A., "Focusing Properties and Operation of a Hemiellipsoidal Mirror Infrared Reflectometer," *Radiative Transfer and Thermal Control*, edited by A. M. Smith, Vol. 49, Progress in Astronautics and Aeronautics, AIAA, New York, 1976, pp. 47–66.

[4]Wood, B. E., and Smith, A. M., "Infrared Reflectance and Refractive Index of Condensed Gas Films on Cryogenic Mirrors," *Thermophysics and Thermal Control*, edited by R. Viskanta, Vol. 65, Progress in Astronautics and Aeronautics, AIAA, New York, 1979, pp. 22–38.

[5]Neu, J., "Hemispherical Mirror Increases Accuracy of Reflectometer," *Laser Focus World*, Vol. 32, No. 4, 1996, pp. 141–143.

[6]Menefee, R. F., "Time-Resolved Target and Plume Optical Properties Measurements During Laser Interactions: Final Report," Antropix Corp., Woodlands, TX, Dec. 1991.

[7]Helgeson, R., "MATTER.DAT Surface Materials Data Compilation," Tracor GIE Corp., GIE-TN-92-013, Provo, UT, 1992.

[8]Sala, A., *Radiant Properties of Materials, Tables of Radiant Values for Black Body and Real Materials*, Elsevier Science, New York, 1986.

[9]Freeman, R., "Independent Verification of Temperature-Dependent Reflectance of Aerospace Materials (TRAM) Laboratory Reflectance Measurements," Science Applications International Corp., Albuquerque, NM, Memorandum to N. Morley, AFRL/DEPE, Kirtland AFB, NM, Sept. 1998.

[10]Wang, C.-C., and Hubka, W. F., *A Material Properties Library for Laser Vulnerability Studies*, Science Applications International Corp., Golden, CO, Feb. 1983.